Structural and Dielectric Properties of $(Bi_{1-x}Ba_x)(Fe_{1-x}Ti_x)O_3$ Multiferroic Ceramics

Authors: T.- H. Wang, C.- S. Tu, V. Hugo Schmidt, R. R. Chien, and Y. Ding

This is an Accepted Manuscript of an article published in Ferroelectrics on 2014, available online: http://www.tandfonline.com/10.1080/00150193.2014.922822.

T.-H. Wang, C.-S. Tu, V.H. Schmidt, R.R. Chien, and Y. Ding, “Structural and dielectric properties of (Bi 1-x Ba x)(Fe 1-x Ti x)O 3 multiferroic ceramics,” Ferroelectrics 470, 52-59 (2014). doi: 10.1080/00150193.2014.922822.

Structural and Dielectric Properties of $(Bi_{1-x}Ba_x)(Fe_{1-x}Ti_x)O_3$ Multiferroic Ceramics

T.-H. WANG,[1] C.-S. TU,[1,*] V. H. SCHMIDT,[2] R. R. CHIEN,[2] AND Y. DING[1,3]

[1]Graduate Institute of Applied Science and Engineering, Fu Jen Catholic University, Taipei 24205, Taiwan
[2]Department of Physics, Montana State University, Bozeman, MT 59717, USA
[3]Teaching Center of Natural Sciences, Minghsin University of Science and Technology, Hsinchu 30401, Taiwan

Phase transitions, dielectric permittivity, and conductivity of $(Bi_{1-x}Ba_x)(Fe_{1-x}Ti_x)O_3$ ($x = 0.05$ and 0.1) [BFO-(Ba,Ti)] multiferroic ceramics have been studied as functions of temperature and frequency. In situ *synchrotron x-ray diffraction revealed rhombohedral–cubic transitions in the temperature ranges 760–780°C in BFO-5%(Ba,Ti), and 720–750°C in BFO-10%(Ba,Ti). A one-dimensional barrier model with intrinsic barriers B every lattice constant* a *and extrinsic barriers $B + \Delta$ is introduced to describe the dielectric response and conductivity. This work revealed that (Ba,Ti) substitutions can enhance the intrinsic barriers and reduce the hopping rate of charge carriers, thereby giving the desired effect of decreasing the conductivity.*

Keywords BFO-(Ba,Ti); phase transition; dielectric permittivity; conductivity; barrier model

I. Introduction

Multiferroic $BiFeO_3$ possesses a coupling interaction between ferroelectric (FE) and antiferromagnetic (AFM) parameters, which attracted much attention in recent years. This magnetoelectric coupling can be used in applications of multifunctionalities that can modulate polarization and magnetization by using external magnetic and electric fields, respectively. The crystallographic structure of $BiFeO_3$ is a rhombohedral structure with lattice constants of $a = 3.96$ Å and $\alpha_R = 89.4^o$ [1] at room temperature. BFO has a relatively high antiferromagnetic (AFM)-paramagnetic (PM) Néel temperature at $T_N =$ 347–397°C (620–670 K) and FE Curie temperature at $T_C =$ 807–877°C (1080–1150 K) [2–6].

Second phases and current leakage are the main concerns in synthesis of $BiFeO_3$ ceramics, which can affect dielectric, ferroelectric, and magnetic properties. The high

electric leakage of $BiFeO_3$ materials is attributed to the reduction of Fe ions ($4Fe^{3+} + 2O^{2-} \rightarrow 4Fe^{2+} + O_{2g}$) during the high-temperature sintering process, thereby creating oxygen vacancies for charge compensation [7, 8]. Most reported BFO ceramics exhibit a relatively small FE spontaneous polarization [9]. To enhance FE and magnetic properties, many studies have focused on substituted BFO ceramics with various ion substitutions in the A or B sites of the perovskite structure [10–12].

Though $(Bi_{1-x}Ba_x)(Fe_{1-x}Ti_x)O_3$ ceramics have been studied in recent years, their phase transition, dielectric response, conductivity, and magnetoelectric coupling properties still lack consistency and are not fully understood. The main focus of this work is to study phase transitions of $(Bi_{1-x}Ba_x)(Fe_{1-x}Ti_x)O_3$ ceramics (x = 0.05 and 0.1) by *in-situ* high-resolution synchrotron x-ray diffraction (XRD) and dielectric permittivity. In addition, a one-dimensional barrier model was introduced to explain the low-frequency conductivities and dielectric maxima behavior upon heating.

II. Experimental Procedure

The $(Bi_{1-x}Ba_x)(Fe_{1-x}Ti_x)O_3$ ceramics were prepared by the solid state reaction method under various sintering temperatures and dwell time. For synthesis of $(Bi_{1-x}Ba_x)(Fe_{1-x}Ti_x)O_3$ ceramics, the mixed powders underwent the following chemical reaction:

$$(1-x)Bi_2O_3 + (1-x)Fe_2O_3 + (2x)BaCO_3 + (2x)TiO_2 \rightarrow 2(Bi_{1-x}Ba_x)(Fe_{1-x}Ti_x)O_3 + (2x)CO_2 \quad (1)$$

The dried starting powders of Bi_2O_3, Fe_2O_3, $BaCO_3$, and TiO_2 (purity $\geq$ 99.0%) were weighed in exact ratio, and then mixed in an agate mortar for more than 24 hrs with alcohol as a medium. The mixture was dried before calcining at 800°C for 3 hrs. A high-energy-ball-milling method by a Retsch PM100 planetary mill was used to reduce the particle size of the calcined powders [10]. The nano-scale calcined powders were mixed with polyvinyl acetate as a binder for granulation. The ground mixture was pressed into 1.0 cm-diameter disks, which were sintered at 870°C for 1 hr for $(Bi_{0.95}Ba_{0.05})(Fe_{0.95}Ti_{0.05})O_3$ [BFO-5%(Ba,Ti)] ceramics and at 940°C for 3 hrs for $(Bi_{0.9}Ba_{0.1})(Fe_{0.9}Ti_{0.1})O_3$ [BFO-10%(Ba,Ti)] ceramics. The densities of optimal $(Bi_{1-x}Ba_x)(Fe_{1-x}Ti_x)O_3$ ceramics are more than 90% of the theoretical densities.

In-situ high-resolution synchrotron XRD was performed at the National Synchrotron Radiation Research Center (in Taiwan) with photon energy of 8.0 keV (λ = 1.550 Å). A Wayne-Kerr Analyzer PMA3260A was used to obtain the real (ε') and imaginary (ε'') parts of dielectric permittivity. The dielectric loss is defined by $\tan\delta = \varepsilon''/\varepsilon'$.

III. Results and Discussion

Figure 1 shows *in-situ* temperature-dependent high-resolution synchrotron (110) XRD reflections of BFO-5%(Ba,Ti) and BFO-10%(Ba,Ti) ceramics upon heating. At room temperature, the two-peak splitting in BFO-5%(Ba,Ti) and BFO-10%(Ba,Ti) ceramics suggests a rhombohedral phase, because two *d* spacings are expected from the (110) reflection for a rhombohedral unit cell according to the lattice equation;

$$\frac{1}{d^2} = \frac{(h^2+k^2+l^2)\sin^2\alpha + 2(hk+kl+hl)(\cos^2\alpha - \cos\alpha)}{a_R^2(1-3\cos^2\alpha+2\cos^3\alpha)} \quad (2)$$

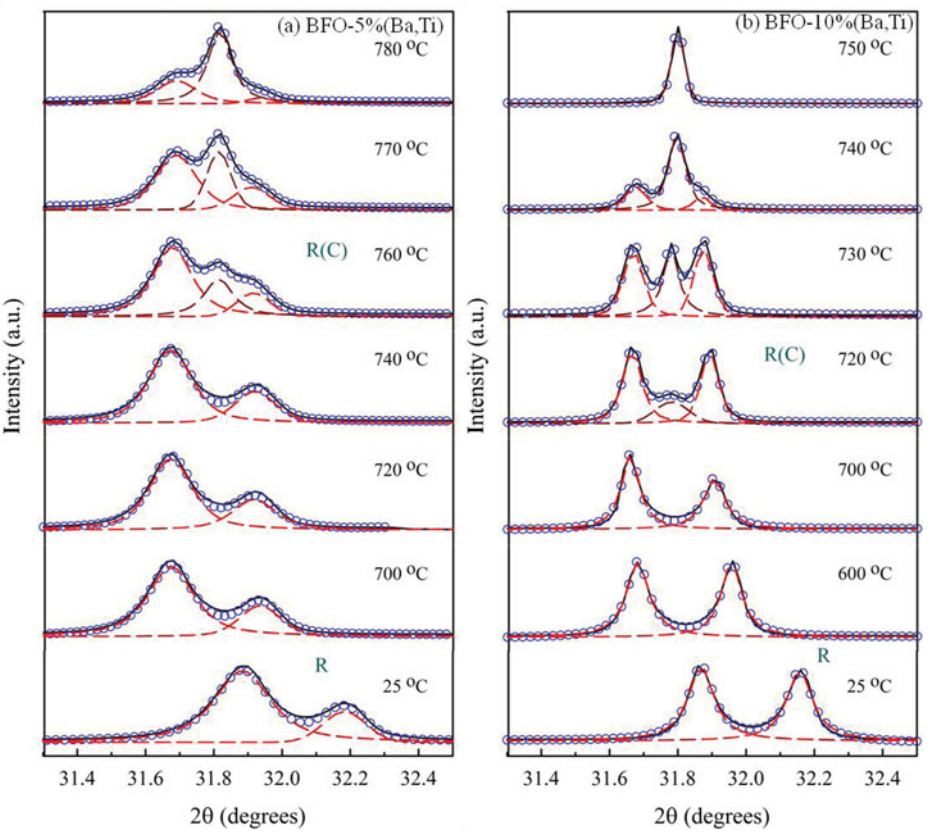

Figure 1. (110) synchrotron XRD of (a) BFO-5%(Ba,Ti) and (b) BFO-10%(Ba,Ti) ceramics upon heating.

where (*h, k, l*) and (a_R, α) are the crystallographic orientation and lattice parameters of the rhombohedral unit cell, respectively [13]. BFO exhibits a transition sequence of rhombohedral (R)–orthorhombic (O)–cubic (C) phases near 820 and 850°C, respectively [14]. These structural transitions are consistent with the result of powder neutron diffraction [15]. Upon heating, the (110) reflection of BFO-5%(Ba,Ti) exhibits a triple-splitting, indicating a gradual R-C transition. R(C) phase coexistence appears near 760°C as shown in Fig. 1(a), and the C phase predominates at 780°C. For BFO-10%(Ba,Ti), the R(C) phase coexistence begins to appear near 720°C, and the triple-splitting peaks from the R(C) phase coexistence turn into a single cubic (C) peak near 750°C as shown in Fig. 1(b). In brief, a gradual R-C transition occurs between 760 and ~780°C in BFO-5%(Ba,Ti), and 720 and 750°C in BFO-10%(Ba,Ti).

Figure 2 shows temperature-dependent lattice parameters calculated from the (110) XRD reflections. A local minimum in rhombohedral distortion angle α_R occurs in BFO-5%(Ba,Ti) and BFO-10%(Ba,Ti) in the regions of 300–400°C. A similar local minimum of α_R was also observed near T_N in BFO [16,17]. This local minimum in α_R indicates a position shift (or distortion) of the Bi^{3+} cation, which gradually reaches a maximum distortion as temperature approaches T_N. This confirms a coupling between ferroelectric and magnetic order parameters near T_N, and is also responsible for the broad frequency-dependent dielectric maxima as shown in Fig. 3.

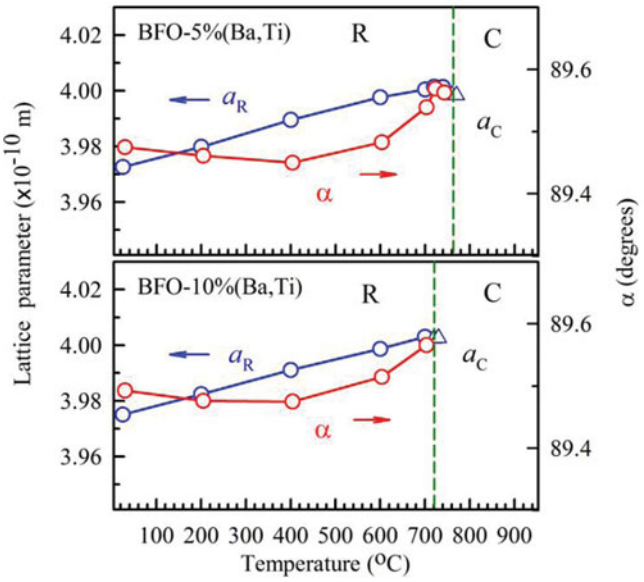

Figure 2. Temperature-dependent lattice parameters of (a) BFO-5%(Ba,Ti) and (b) BFO-10%(Ba,Ti) ceramics. a_R, α_R, and a_C are lattice parameters of rhombohedral and cubic structures. The lattice parameters were calculated based on the pseudo-cubic lattice.

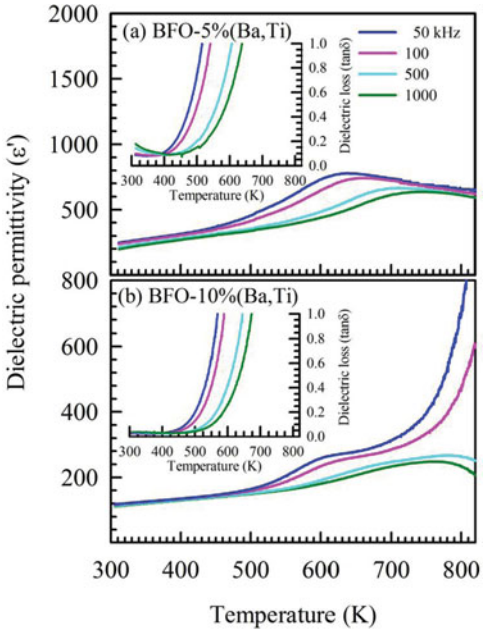

Figure 3. Frequency- and temperature-dependent dielectric permittivity (ε') and loss (tan δ) of (a) BFO-5%(Ba,Ti) and (b) BFO-10%(Ba,Ti) ceramics upon heating.

The temperature- and frequency-dependent dielectric permittivity (ε') and dielectric loss ($\tan\delta = \varepsilon''/\varepsilon'$) of BFO-5%(Ba,Ti) and BFO-10%(Ba,Ti) ceramics are given in Fig. 3. The real part ε' of dielectric permittivity of BFO-5%(Ba,Ti) and BFO-10%(Ba,Ti) are respectively about 200 and 110 at room temperature for measuring frequency of 1 MHz. In addition, the dielectric permittivity of BFO-10%(Ba,Ti) exhibits less frequency dispersion in the lower temperature region than the BFO-5%(Ba,Ti), indicating that (Ba,Ti) substitution can enhance homogeneity of dielectric response in the BFO ceramic matrix.

The temperature (T_m) corresponding to the dielectric maximum exhibits a broad frequency dispersion as shown in Fig. 3. For BFO, T_m shifts from ~700 K at 50 kHz to ~750 K at 1 MHz [14]. This T_m range shifts toward lower temperatures in 5 and 10 mol% (Ba,Ti) substitutions at frequencies of 50 kHz-1 MHz. This frequency dependent dielectric maximum is likely activated by the AFM–PM transition which takes place at the Néel temperature (T_N). This AFM-PM transition also associates with a local minimum in rhombohedral distortion angle α_R near T_N [16], which correlates to the changes in relative positions of Bi^{3+} and Fe^{3+} ions in the perovskite structure. In addition, the neutron scattering result of BFO revealed changes of distortion and strain in oxygen octahedral (FeO_6) at T_N caused by the magnetoelectric and/or magnetoelastic couplings [18].

The dielectric loss ($\tan\delta$) values of BFO-5%(Ba,Ti) and BFO-10%(Ba,Ti) ceramics are respectively about 0.05–0.15 and 0.02–0.03 at room temperature for measuring frequencies of 50 kHz-1 MHz, indicating that 10 mol% (Ba,Ti) substitution can efficiently reduce electric conductivity. The dielectric losses of BFO and BFO-(Ba,Ti) exhibit an exponential upturn above ~570 K with magnitude proportional to $1/f$. These high-temperature dielectric phenomena are likely initiated by the hopping conductivity associated with the random barrier distribution [19].

Figure 4 shows the frequency- and temperature-dependent conductivity σ' and dielectric permittivity ε' for $f = 10$–1000 kHz. The dashed lines are fits of the one-dimensional barrier model for BFO, BFO-5%(Ba,Ti), and BFO-10%(Ba,Ti) ceramics for $f = 10$–1000 kHz. The one-dimensional barrier model is given in the next section. Good qualitative fits of conductivity σ' and dielectric permittivity ε' are obtained in the high-temperature region with $d = 40$ and 30 nm for BFO and substituted BFO. BFO-5%(Ba,Ti) and BFO-10%(Ba,Ti) have higher intrinsic barriers B than BFO, indicating that (Ba,Ti)-substituted can reduce the hopping activity of the charge carriers.

IV. One-Dimensonal Barrier Model

To understand the conductivity and dielectric response in terms of temperature and frequency, a one-dimensional barrier model was introduced as illustrated in Fig. 5, in which B (in temperature units) represents the intrinsic barriers spaced a distance a apart, where a is of the order of a lattice constant. $B + \Delta$ are extrinsic barriers spaced a distance d apart. The attempt frequency for crossing the barriers is estimated by using $\nu = k\Theta/h$, where k, Θ, and h are the Boltzmann constant, Debye temperature, and Planck's constant. We chose $\Theta = 300$ K, *i.e.* $\nu = 6.25 \times 10^{12}$Hz. The complex ac conductivity $\sigma(\omega, T) = \sigma' + i\sigma''$can be defined as;

$$\sigma(\omega, T) = (J + \partial D/\partial t)/ < E > \tag{3}$$

J and $\partial D/\partial t$ are conduction current density and the displacement current density. $<E$ is the spatially averaged measured field, whereas E is position-dependent. The complex dielectric

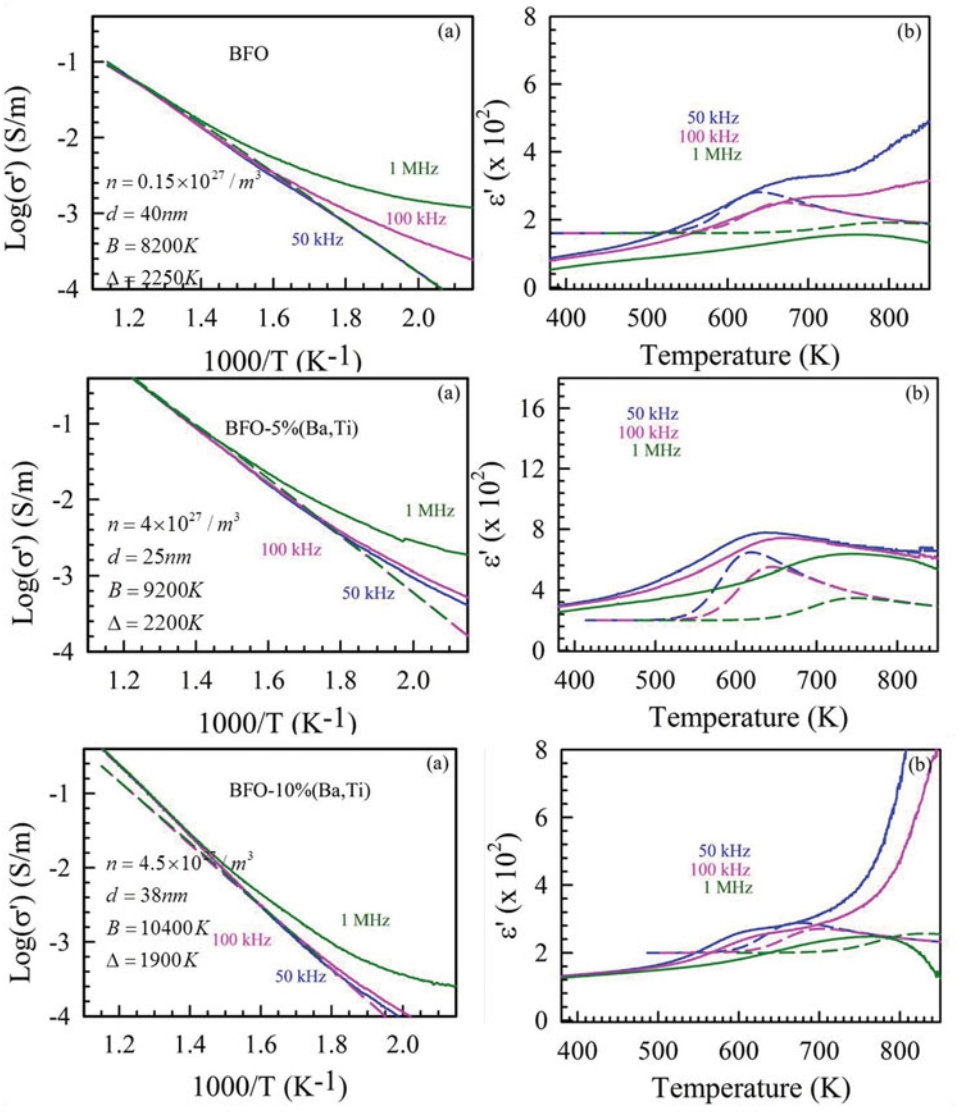

Figure 4. (a) Conductivities (σ') and (b) fitting lines of barrier model to permittivity (dashed lines) for measuring frequencies $f = 10$–1000 kHz.

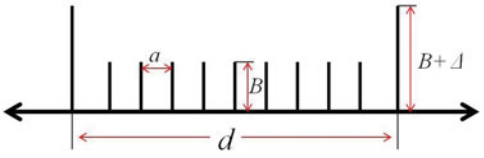

Figure 5. One-dimensional barrier model with intrinsic barriers B at spacing a, and extrinsic barriers $B + \Delta$ at spacing d.

permittivity $\varepsilon(\omega,\ T) = \varepsilon' - i\varepsilon''$is related to ac conductivity by

$$\varepsilon' = \sigma''/\varepsilon_o\omega,\ \varepsilon'' = \sigma'/\varepsilon_o\omega \tag{4}$$

where ε_o is the MKS constant 8.854×10^{-12} C^2/Nm^2. For high-frequency conductivity, we assume conductivity with a temperature-independent carrier density n and carrier charge q. The high-frequency conductivity $\sigma_\infty = J/E$, considering that the number of carrier per unit area in a unit-cell layer on each side of a barrier layer is na and their attempt frequency for crossing the barrier is ν, can be expressed by;

$$\sigma_\infty = q\nu na\{e^{(-kB+\frac{1}{2}qEa)/kT} - e^{(-kB-\frac{1}{2}qEa)/kT}\}/E \cong (q^2\nu na^2/kT)e^{-B/T} \\ (nq^2a^2\Theta/hT)e^{-B/T} \tag{5}$$

By using Eqs. (3)–(5) and carrying considerable algebraic calculations, we obtain [20]

$$\sigma = \sigma' + i\sigma'' = \sigma_\infty\{b\cosh(b) + r\sinh(b) + it\tan\phi[r\sinh(b) + e^{\Delta/T}b\cosh(b)]\} \bullet \\ \{r\sinh(b) + be^{\Delta/T}\cosh(b) - (e^{\Delta/T}-1)\cos\phi e^{-i\phi}(b\cosh b - \sinh b)\}^{-1} \tag{6}$$

where $r = d/a$, $b = \alpha d/2$, $\varepsilon_\infty = \varepsilon_o\varepsilon'_\infty$, and $\phi = \tan^{-1}(\omega\varepsilon_\infty/\sigma_\infty)$. The lattice constant of a = 0.395 was estimated from the room-temperature XRD result.

As shown in Fig. 4, the conductivities σ' were fitted fairly well by using Eq. (6), from which parameters of ε'_∞, n, d, B, and Δ were obtained. The extrinsic-barrier distances of d = 20–40 nm for BFO, BFO-5%(Ba,Ti), and BFO-10%(Ba,Ti) are smaller than the grain size (∼1–5 μm), implying possible internal boundaries inside grain and defects. The discrepancy between the model and data could be due to other conductivity contributions, such as having both ionic and electronic conductivity, and to actual higher barriers having a distribution of spacing d and heights B + Δ.

V. Conclusions

In conclusion, high-density BFO-5%(Ba,Ti) and BFO-10%(Ba,Ti) ceramics have been synthesized by using the solid-state-reaction method. A gradual rhombohedral-cubic transition occurs between 760 and ∼780°C in BFO-5%(Ba,Ti), and 720 and 750°C in BFO-10%(Ba,Ti). The Curie temperature shifts toward lower temperature as (Ba,Ti) substitutions increase. A local minimum in rhombohedral distortion angle α_R was revealed near 300-400°C in BFO-5%(Ba,Ti) and BFO-10%(Ba,Ti) ceramics, indicating the position distortion of Bi^{3+} reaches the maximum near T_N. This suggests a magnetoelectric coupling near T_N, which is responsible for the broad frequency dispersion in dielectric maxima. A one-dimensional barrier model can qualitatively fit the low-frequency upturn in dielectric response and conductivity upon heating. The (Ba,Ti) substitutions in BFO can enhance dielectric response and intrinsic barriers, which considerably reduces the hopping activity of the charge carriers.

Funding

This work was supported by National Science Council of Taiwan Grant Nos. 97-2112-M-030-003-MY3 and NSC 100-2112-M-030 -002 -MY3.

References

1. F. Kubel, and H. Schmid, Structure of a ferroelectric and ferroelastic monodomain crystal of the perovskite $BiFeO_3$. *Acta Crystallogr.* **B46**, 698–702 (1990).
2. J. R. Teague, R. Gerson, and W. J. James, Dielectric hysteresis in single crystal $BiFeO_3$. *Solid State Commun.* **8**, 1073–1074 (1970).
3. P. Fischer, M. Polomska, I. Sosnowska, and M. Szymański, Temperature dependence of the crystal and magnetic structures of $BiFeO_3$. *J. Phys. C* **13**, 1931–1940 (1980).
4. M. M. Kumar, and V. R. Palkar, Ferroelectricity in a pure $BiFeO_3$ ceramic. *Appl. Phys. Lett.* **76**, 2764 (2000).
5. J. C. Chen, and J. M. Wu, Dielectric properties and ac conductivities of dense single-phased $BiFeO_3$ ceramic. *Appl. Phys. Lett.* **91**, 182903 (2007).
6. B. Ramachandran, and M. S. Ramachandra Rao, Low temperature magnetocaloric effect in polycrystalline $BiFeO_3$ ceramics. *Appl. Phys. Lett.* **95**, 142505 (2009).
7. V. R. Palkar, J. John, and R. Pinto, Observation of saturated polarization and dielectric anomaly in magnetoelectric $BiFeO_3$ thin films. *Appl. Phys. Lett.* **80**, 1628 (2002).
8. Y. P. Wang, L. Zhou, M. F. Zhang, X. Y. Chen, J. M. Liu, and Z. G. Liu, Room-temperature saturated ferroelectric polarization in $BiFeO_3$ ceramics synthesized by rapid liquid phase sintering. *Appl. Phys. Lett.* **84**, 1731 (2004).
9. I. H. Ismailzade, I. M. Ismailov, A. I. Alekberov, and F. M. Salaev, Investigation of the magnetoelectric $(ME)_H$ effect in solid solutions of the systems $BiFeO_3$-$BaTiO_3$ and $BiFeO_3$-$PbTiO_3$. Phys. Stat. Sol. (a) **68**, K81–85 (1980).
10. S. Karimi, I. M. Reaney, I. Levin, and I. Sterianou, Nd-doped $BiFeO_3$ ceramics with antipolar order. *Appl. Phys. Lett.* **94**, 112903 (2009).
11. K. Singh, Kotnala R. K., and M. Singh, Study of electric and magnetic properties of $(Bi_{0.9}Pb_{0.1})(Fe_{0.9}Ti_{0.1})O_3$ nanomultiferroic system. *Appl. Phys. Lett.* **93**, 212902 (2008).
12. P. Pandit, S. Satapathy, P. K. Gupta, and V. G. Sathe, Effect of coalesce doping of Nd and La on structure, dielectric, and magnetic properties of $BiFeO_3$. *J Appl. Phys.* **106**, 114105 (2009).
13. B. D. Cullity, Elements of X−ray diffraction, Addison-Wesley Publishing; 1978.
14. T. H. Wang, C. S. Tu, H. Y. Chen, Y. Ding, T. C. Lin, Y. D. Yao, V. H. Schmidt, and K. T. Wu, Magnetoelectric coupling and phase transition in $BiFeO_3$ and $(BiFeO_3)_{0.95}(BaTiO_3)_{0.05}$ ceramics. *J. Appl. Phys.* **109**, 044101 (2011).
15. D. C. Arnold, K. S. Knight, G. Catalan, S. A. T. Redfern, J. F. Scott, P. Lightfoot, and F. D. Morrison, The β-to-γ transition in $BiFeO_3$: a powder neutron diffraction study. *Advanced Functional Materials* **20**, 2116–2123 (2010).
16. A Singh, V. Pandey, R. K. Kotnala, and D. Pandey, Direct evidence for multiferroic magnetoelectric coupling in $0.9BiFeO_3$-$0.1BaTiO_3$. *Phys. Rev. Lett.* **101**, 247602 (2008).
17. A. Palewicz, R. Przenioslo, I. Sosnowska, and A. W. Hewat, Atomic displacements in $BiFeO_3$ as a function of temperature: neutron diffraction study. *Acta Cryst. B* **63**, 537–544 (2007).
18. P. Fischer, M. Polomska, I. Sosnowska, and M. Szymanski, Temperature dependence of the crystal and magnetic structures of $BiFeO_3$. *J. Phys. C* **13**, 1931–1940 (1980).
19. V. H. Schmidt, G. F. Tuthill, C. S. Tu, T. V. Schogoleva, and S. C. Meschia, Conductivity across random barrier distribution as origin of large low-frequency dielectric peak in perovskite crystals and ceramics. *J. Phys. Chem. Solid* **57**, 1493–1497 (1996).
20. C. S. Tu, W. C. Yang, V. H. Schmidt, and R. R. Chien, Origins of dielectric response and conductivity in $(Bi_{1-x}Nd_x)FeO_3$ multiferroic ceramics. *J. Appl. Phys.* **110**, 114114 (2011).